Superconducting pairing mechanism in CeCoIn$_5$ revisited

T. J. Reber,[1] J. D. Rameau [1] C. Petrovic,[1] Hasnain Hafiz [2] M. Lindroos,[2,3] A. Bansil,[2] and P. D. Johnson [1]

[1]*Condensed Matter Physics and Materials Science Division, Brookhaven National Laboratory, Upton, New York 11973, USA*
[2]*Physics Department, Northeastern University, Boston, Massachusetts 02115, USA*
[3]*Computational Physics Laboratory, Tampere University, Tampere, Finland*

Spectroscopic Imaging Scanning Tunneling Microscopy (SI-STM) measurements have previously been applied to the study of the heavy-fermion system CeCoIn$_5$ to examine the superconducting gap structure and band dispersions via quasiparticle intereference. Here we directly measure the dispersing electron bands with angle-resolved photoelectron spectroscopy (ARPES) and compare with first-principles electronic structure calculations. By autocorrelating the ARPES-resolved bands with themselves we can measure the potential q vectors and discern exactly which bands the STM is measuring. We find that the STM results are dominated by scattering associated with a cloverleaf shaped band centered at the zone corners. This same band is also a viable candidate to host the superconducting gap. The electronic structure calculations indicate that this region of the Fermi surface involves significant contributions from the Co d electrons, an indication that the superconductivity in these materials is more three dimensional than that found in the related unconventional superconductors, the cuprates and the pnictides.

I. INTRODUCTION

The heavy-fermion superconductors represent one of the first families of superconductors discovered that display unconventional superconductivity or anisotropic superconducting energy gaps [1]. As such, these materials, alongside the cuprates, have proved important testbeds for investigating the emergence of complex behavior in correlated electron systems. With the highest superconducting transition temperature T_c of all the non-plutonium-based heavy-fermion superconductors, CeCoIn$_5$ has garnered much attention since its discovery two decades ago [2]. Electronic structure computations find three distinct bands crossing the Femi energy, E_F [3–5]. A key challenge in these materials has been the interplay of local and itinerant behavior. In particular, the Ce $4f$ electrons are generally considered localized at high temperatures but more itinerant following hybridization with the itinerant electrons at low temperatures [6]. Indeed, participation of the $4f$ levels in the formation of the Fermi surface takes place only at low temperatures through this hybridization, and dynamical mean field theory (DMFT) calculations predict that as a result the Fermi surface will be enlarged below the Kondo transition [7]. Direct studies of the band structure via angle-resolved photoemission spectroscopy (ARPES) [8] are generally in accord with these theoretical predictions [9–13]. However, ARPES studies on the transition from localized to itinerant behavior have produced mixed results. One study reports a high level of localization persisting at a temperature of 25 K, well below the Kondo transition [10], $T_K = 40$ K, while another study reports evidence of itineracy at temperatures well above the Kondo temperature [13]. The latter study also reported a temperature-dependent Fermi surface for CoCeIn$_5$ although a temperature-independent Fermi surface was reported for the related material YbRh$_2$Si$_2$ [14].

Spectroscopic Imaging Scanning Tunneling Microscopy (SI-STM) experiments based on the quasiparticle interference (QPI) analysis have also purported to deduce the band structure and hybridization of the conduction and heavy-fermion bands [15–18]. In comparing the two techniques, ARPES and SI-STM, ARPES has the advantage of being able to measure band dispersions and Fermi surfaces directly in k space with high-energy and momentum resolution. SI-STM, on the other hand, has the advantage of being able to measure the anisotropy and magnitude of the hybridization and superconducting gaps with very high-energy resolution. Both spectroscopies thus bring important information to the problem.

Diverging from earlier ARPES results, the SI-STM studies of the dispersing bands uniformly identified a single hole pocket at the center of the Brillouin zone. In studies of the superconducting gap, SI-STM identified an anisotropic gap with an order parameter of $d_{x^2-y^2}$ symmetry [16–18]. In one of the latter studies, it was suggested that since the observed superconducting gap existed predominantly at high q values, it must primarily form on the heavy band associated with the f electrons [16]. This is an interesting suggestion. ARPES studies universally report that any hybridization of the Ce f levels with the conduction band takes place around the zone center [11,13]. QPI reflects the scattering from momentum $\boldsymbol{k_1}$ to $\boldsymbol{k_2}$, where the sacattering vector $\boldsymbol{q} = \boldsymbol{k_1} - \boldsymbol{k_2}$. If $\boldsymbol{q}$ is large and $\boldsymbol{k_1}$ is small (center of the zone), then $\boldsymbol{k_2}$ must be large. We investigate this proposition further using ARPES to measure the band structure of CeCoIn$_5$. By comparing with parallel first-principles electronic structure calculations we offer

greater insight into the orbital character of various pieces of the Fermi surface. Then, recognizing that autocorrelation of the ARPES (AC ARPES) spectra can, in principle, be mapped onto the q-space structure determined via a QPI analysis of the STM spectra, we examine in detail the involvement of the heavy fermions as suggested in the SI-STM studies. Thus our approach is to compare our experimentally measured dispersions directly with first-principles electronic structure calculations that identify the orbital character of the different regions of the Fermi surface. By using a tight-binding fit to the bands, we analyze SI-STM studies, and identify the bands from which the SI-STM-observed q vectors originate. Our analysis suggests that if the pairing in CeCoIn$_5$ involves the heavy Ce $4f$ levels, it is those f levels that hybridize with the out-of-plane In and Co orbitals and therefore the localized Co $3d$ electrons must play a more significant role in the onset of unconventional superconductivity in CeCoIn$_5$ than previously recognized.

II. METHODS

Single crystals of CeCoIn$_5$ were synthesized from an In flux by combining stoichiometric amounts of Ce and Co with excess In in an alumina crucible and encapsulating the crucible in an evacuated quartz ampoule. More details are presented elsewhere [2]. Samples were cleaved in the experimental chamber with an onboard cleaver using an attached razor blade [19]. Surfaces were then raster scanned using low-resolution ARPES to identify bright electron emission points corresponding to high-quality cleaved surfaces.

Photoemission data were taken at the SIS beamline at the Swiss Light Source using a Scienta R4000 analyzer. The energy resolution varied with photon energy but was generally 10–20 meV. The beamline offers the possibility of using either linearly or circularly polarized incident light. It is now well established that investigation of the heavy fermions reflecting the Ce $4f$ levels is best accomplished using a photon energy corresponding to the $4d \rightarrow 4f$ resonance of Ce, namely, 121 eV [20], which is the photon energy used in this study. Note that at this photon energy the sampled k_z will correspond to excitation close to the Γ-M-Z sector of the Brillouin zone. We show in the Supplemental Material the demonstration of the resonant photoemission as reproduced in the present study [21].

Electronic structure calculations were carried out within the GGA $+ U$ scheme using the full-potential linearized augmented plane-wave (FP LAPW) [22] scheme as implemented in the WIEN2K package [23]. Because the gradient corrections to the local spin-density approximation are important for treating magnetic properties of transition metals [24], the exchange-correlation effects were accounted for by using the generalized-gradient approximation (GGA) with Perdew-Burke-Ernzerhof (PBE) functional [25]. Computations were carried out on a $10 \times 10 \times 10$ k mesh in the first Brillouin zone (BZ) with a plane wave cutoff $k_{max} = 8$ in order to obtain well-converged energies and electronic structures.

III. RESULTS

Figure 1 shows the crystal structure of CeCoIn$_5$ that is seen to consist of planes of CeIn$_3$ interspersed with layers of CoIn$_2$
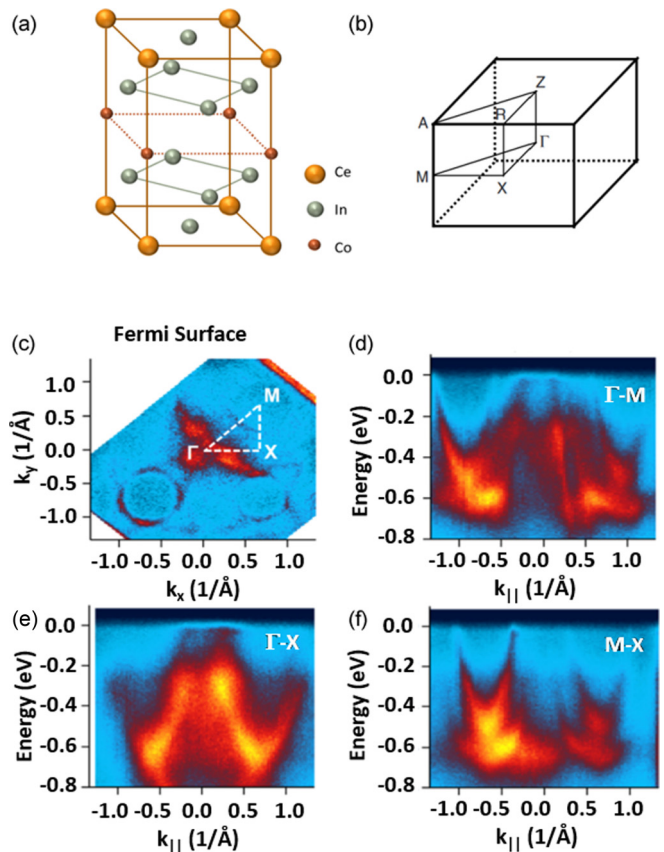

FIG. 1. (a) Crystal structure of CeCoIn$_5$ where the individual atoms are identified and (b) the associated Brillouin zone. Two momentum planes in the BZ, which are discussed in the text (ΓXM and ZAR), defined by $z = 0$ for Γ and $z = \pi$ for Z, are highlighted. (c) Experimental Fermi surface corresponding to the ΓXM plane and (d)–(f) experimental dispersions along the high-symmetry directions Γ-M, Γ-X, and M-X.

and the associated BZ, along with the ΓXM ($k_z = 0$) and ZAR ($k_z = \pi$) momentum planes in the BZ. The figure also shows in panel (c) the experimentally measured Fermi surface corresponding to the ΓXM plane, and in panels (d–f) the experimental dispersions along the high-symmetry directions indicated. These measurements, as noted above, were carried out with an incident photon energy of 121 eV to emphasize emission from the Ce f levels associated with momenta corresponding to the the ΓXM plane. Note that the sharp emission in panels (d) and (e) around the chemical potential at the BZ center is characteristic of the $4f$ levels.

Figures 2(a) and 2(b) show the calculated Fermi surface in the ΓXM and ZAR momentum planes [see Fig. 1(b)]. The characteristic cloverleaf pattern in the ΓXM plane is in excellent agreement with the previously reported DMFT-based results in the related CeIrIn$_5$ compound [7]. In ARPES, we can selectively excite from either the ΓXM or the ZAR momentum plane by tuning the incident photon energy. In contrast, SI-STM does not discriminate between excitations from these two planes and the Fermi surface derived from a QPI analysis in one of the SI-STM studies [16] clearly reflects contributions from both planes. Figures 2(c) and 2(d) show the calculated electronic structure at key points in the BZ and the
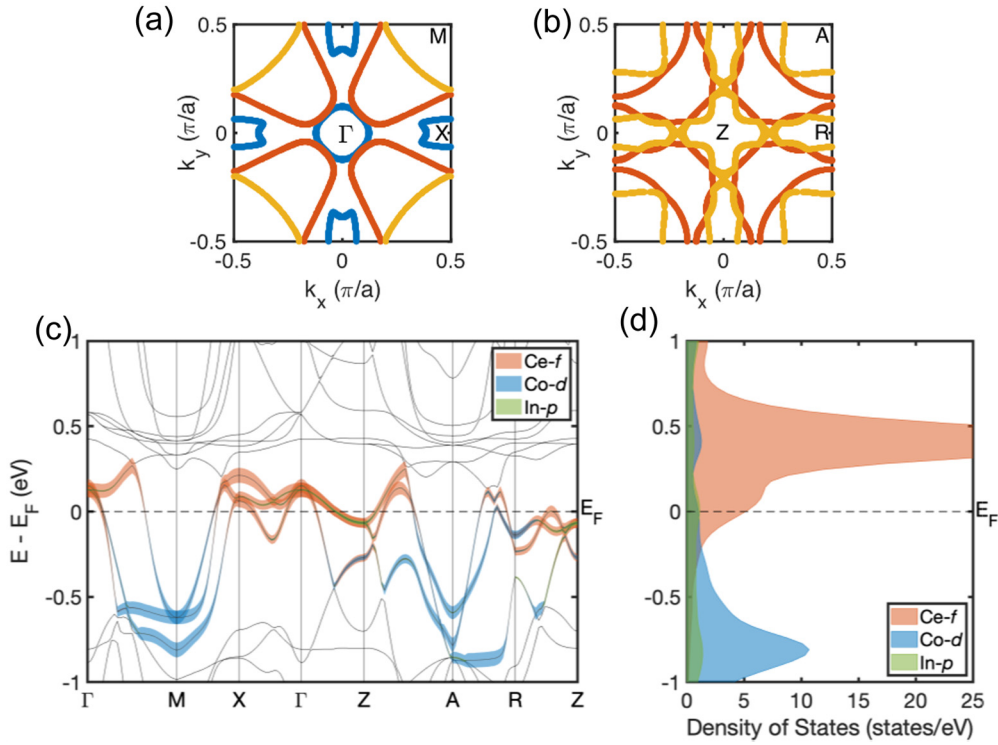
FIG. 2. (a), (b) Calculated Fermi surfaces in the ΓXM and ZAR momentum planes shown in Fig. 1(b). (c) Calculated band structure along high-symmetry lines in the BZ where the bands near the Fermi level are highlighted with their respective orbital characters. (d) Orbital-dependent density of states for the Ce $4f$ (red), Co $3d$ (blue), and In $5p$ (green) bands.

orbital-dependent density of states derived from the Ce $4f$, Co $3d$, and In $5p$ bands. In Fig. 2(d) it is clear that much of the weight of the heavy $4f$ electrons lies well above the chemical potential. However, hybridization with the itinerant electrons brings heavy-fermion behavior to the chemical potential, allowing its participation in defining the topology of the Fermi surface. Earlier calculations indicate that in the vicinity of the chemical potential the f electrons primarily reflect the $J = 5/2$ multiplet [5,26]. In the Supplemental Material we show circular dichroism ARPES results that offer support to this observation [21]. Note that the weight of the Co $3d$ electrons is also well displaced from the chemical potential but lies at a relatively high binding energy.

In looking at Fig. 2(c) we note that the $4f$ electrons manifest at the Fermi surface throughout the zone reflecting their hybridization with the itinerant electrons. Interestingly, we can see that in the Γ-M direction there is a greater level of hybridization with the Co $3d$ levels and in the Γ-X direction a greater involvement with the In $5p$ levels, the latter reflecting the In atoms in the CeIn$_3$ planes. In the Γ-M direction the out-of-plane In atoms contribute more, along with the out-of-plane Co $3d$ levels. The latter, as previously noted, will be more strongly correlated than the In p levels.

In Fig. 3 we compare our first-principles calculations with our experimentally measured Fermi surface in the ΓMX plane and with the experimentally measured dispersions along the high-symmetry directions Γ-M, Γ-X, and M-X. The chemical potential in the calculation was moved to higher binding energy by approximately 0.1 eV to bring the experiment and theory into full alignment at the M point. No other adjustment was made in either energy or momentum and, as is evident in

the figure, excellent agreement is obtained with the measured dispersions. In the ΓX direction, we show only the calculated contributions from the $4f$ levels right at the Fermi level. However, we do note that, experimentally, the hole pockets away from the center of the zone in the latter direction are observed much farther out in k space, if at all.

In order to do a more detailed comparison with the SI-STM studies we now perform a tight-binding (TB) fit that captures the measured dispersion and which is in overall accord with the first-principles calculations. In particular, we parametrizethe band structure with three bands that capture the behavior observed along all the high-symmetry directions via a relatively simple tight-binding model of the form

$$
\begin{aligned}
E(k) = u - 2t_0\{ & \cos(k_x) + \cos(k_y) - 4t_1\cos(k_x)\cos(k_y) \\
& - 2t_2[\cos(2k_x) + \cos(2k_y)] \\
& - 4t_3[\cos(2k_x)\cos(k_y) + \cos(2k_y)\cos(k_x)] \\
& - 4t_4\cos(2k_x)\cos(2k_y)\},
\end{aligned} \tag{1}
$$

where the parameters are given in Table I.

TABLE I. Parameters used in the TB fit to the measured experimental dispersions using equation (1) in the main text.

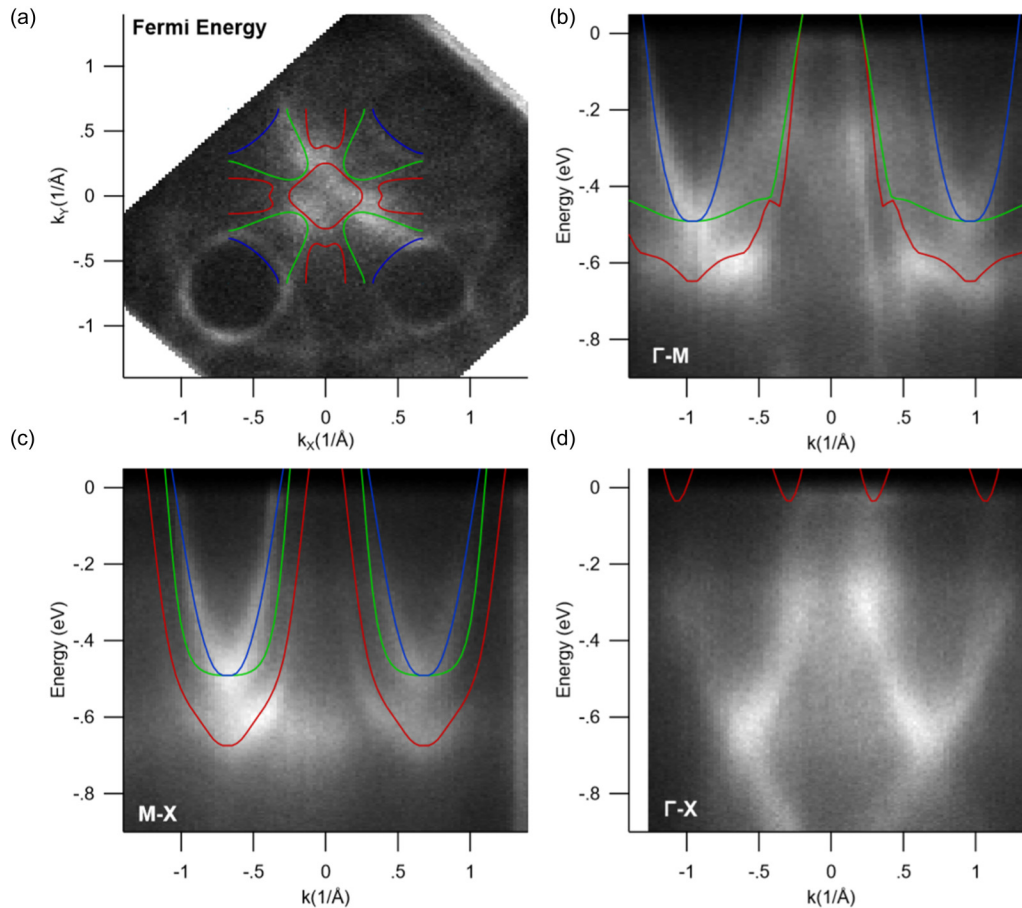| Band	u	t_0	t_1	t_2	t_3	t_4
Red	0.4	t_0	t_1	t_2	t_3	t_4
Blue	0.1	–0.1	0.18	–0.1	0	0
Yellow	–1.125	–0.3	0	–0.1	0.05	–0.01

FIG. 3. Comparison of our first-principles results with the corresponding experimental Fermi surface in the ΓMX plane and the measured dispersions in the high-symmetry directions Γ-*M*, Γ-*X*, and *M*-*X*. The chemical potential in the calculations is adjusted by approximately 0.1 eV to give full alignment. Only the calculated contributions from the $4f$ levels at the Fermi level are shown along the ΓX direction.

In Fig. 4 we compare our experimental dispersions with the tight-binding model of Eq. (1) as well as the results of the earlier SI-STM studies [16,17]. In particular Fig. 4(a) shows the Fermi surface map, with two clear bands centered at the zone corners, a circular electron band and a cloverleaf-shaped electron band. The large spectral weight near the zone center is from the flat f states and obscures the crossing of a third holelike band. All three bands are visible along the Γ-*M* zone diagonal in Fig. 4(b). Along Γ-*X*, only one conduction band is evident but the f states are clear showing they either have their closest approach to, or cross, the Fermi energy near Γ. Finally, along the zone boundary, the two electron bands overlap and show the strongest suggestion of hybridization with the f band near the Fermi energy. Based on this parametrization of the bands, we see good agreement between the Fermi surface observed in the present experiment and those previously observed experimentally and between the present study and the first-principles calculation presented here.

In Figs. 4(e)–4(h) we again show the Fermi surface and dispersions determined experimentally in the present study but now overlayed with the parametrizations determined in the earlier STM studies [16,17]. The STM results show qualitative agreement in that near the zone center there is a holelike band. However, it is does not match the experimental ARPES observation which suggests a much smaller hole pocket. As for

the f state, one proposed parametrization [17] most closely matches our experimental observation even though it never crosses E_F, its closest proximity being near Γ. This finding is in contrast to the other SI-STM interpretation, that the superconducting gap lives on the f states at high k values [16]. For the superconducting gap to form with the f electrons they must cross the Fermi energy. Our data and other data presented elsewhere [11,13] show that if the localized f levels cross the Fermi energy it is near the Γ point.

To better understand how the band structure extracted from SI-STM is so different from that determined in the present study, it is helpful to understand exactly how the STM deduces the band structure. STM is a real-space probe that directly measures the local electron density of states (LDOS). In a material with impurities or vacancies, this density will undulate because incoming electrons with a momentum, k_1, will scatter off of the impurity to an outgoing wave vector, k_2. As noted earlier, these two electronic states will interfere creating a standing wave with a momentum $q = k_1 – k_2$, which can be expressed as

$$I(q) = \int A(k)T(q)A(q - k)dk. \qquad (2)$$

To convert the real-space maps to this momentum transfer space, one simply Fourier transforms the data although
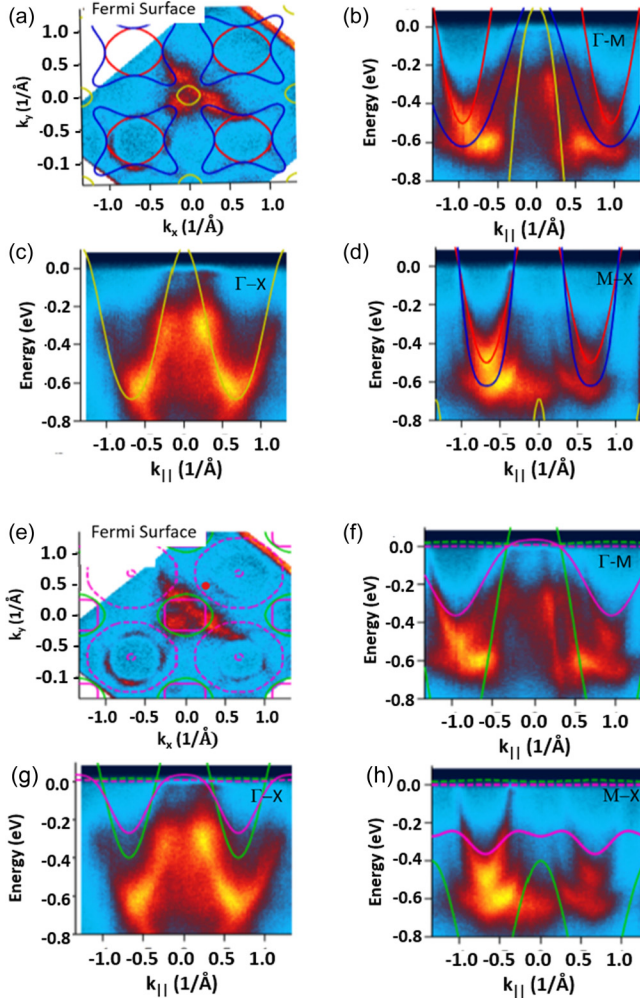
FIG. 4. Comparison of our experimental Fermi surface and measured dispersions with two TB parametrizations. (a)–(d) are based on the parametrization in Eq. (1). (e)–(h) are the same as (a)–(d) except that these panels refer to STM parametrizations in Ref. [16] (magenta lines) and Ref. [17] (green lines).

conversion from q space to k space is an ill-posed inverse problem: Certain ambiguities creep in as a particular model must be chosen. For example, in the studies we are comparing with, it is unclear whether the deduced hole pocket is centered at Γ or at M. However, we do not simply compare our results in k space. ARPES momentum maps can be converted to q space as well. Thus we take our observed band structure, shift it in momentum space by a distance q, and then correlate this with the unshifted band structure, an operation which can be expressed as

$$I(q) = \int A(k)A(q - k)dk. \qquad (3)$$

Note that Eqs. (2) and (3) are not identical. While ARPES can probe all potential scatterings, STM probes only the scattering vectors q that actually occur, so a more complete understanding of a system can be obtained by combining the results from these real- and k-space probes.

Figure 5(a) shows a Fermi surface taken with 121-eV photons with our parametrization of the bands overlaid. The

indistinct and noisy nature of these data precludes direct autocorrelation to convert to q space. Instead, we generate an idealized Fermi surface using our bands assuming an energy broadening of 25 meV [Fig. 5(b)]. Autocorrelating this Fermi surface results in the complex q-space structure shown in Fig. 5(c). While this qualitatively reproduces the stuctures observed in SI-STM studies, it is difficult to identify the contributions from the different regions of the Fermi surface. Instead, we separate out each band and generate the corresponding Fermi surfaces [Figs. 5(d)–5(f)]. The autocorrelations of each Fermi surface in panels (g–i) reveal the q vectors associated with intraband scattering. We can also parse the interband scattering q vectors by cross correlating the bands as shown in panels (j–l). In order to compare with the STM results, we mark on all our q maps the critical q vectors for the conduction band (circle) and the superconducting gap ($\times$) as reported in one of the SI-STM studies [16]. We note that a second SI-STM study reported almost identical q vectors connecting the conduction band [17]. Note that only the blue band has peaks near these critical q vectors and is thus the band the STM experiments are most likely probing. The associated scattering events with $q = (\pm 1, \pm 1)\pi/a_0$ and $q = (\pm 1, 0)\pi/a_0$ [16,17] are shown by the arrows in panel (f), with the solid lines denoting the conduction band and the dashed lines the superconducting gap. We note that the second SI-STM study [17] also reported a third critical q vector for the conduction bands, this also in the $q = (\pm 1, \pm 1)\pi/a_0$ direction. We show the latter as a yellow line in panel (f) where we note that it connects directly the ends of the cloverleaf identified in the present study. In the Supplemental Material we discuss the results of calculations as a function of the binding energy to map the dispersion of the q vectors for various scatterings [21]. Autocorrelation of the blue band is found to generate q vectors that qualitatively match the measured dispersions found in SI-STM studies consistent with our proposal that the STM mainly observes the cloverleaf band, the unusual shape of which would certainly complicate the determination of band structure from the observed q vectors. This insight offers the opportunity for a reinterpretation of the SI-STM results on the superconducting gap in $CeCoIn_5$ and the pairing mechanism in this material.

IV. DISCUSSION

SI-STM analyses of the superconducting gap function point to two characteristic q vectors, a strongly repulsive $q_1 = (\pm 1, \pm 1)\pi/a_0$ and an attractive $q_2 = (\pm 1, 0)\pi/a_0$ [16,18]. It is the repulsive interaction q_1 that results in unconventional superconductivity. The scattering vectors q_1 and q_2 are expected to connect different parts of the Fermi surface with the same sign of the phase for the former and a different sign of the phase for the latter vector. The analysis detailed in the present study lends some weight to this choice of q vectors as evidenced in Figs. 5(f) and 5(i). Our results for autocorrelation of the ARPES-measured electronic dispersion also make it clear that these q vectors reflect intraband scattering on the cloverleaf structure and point to these vectors as the primary route for pairing.

The consensus appears to be that in $CeCoIn_5$ the heavy electrons pair to produce the superconducting state. It is also generally agreed that the heavy electrons reflect hybridization
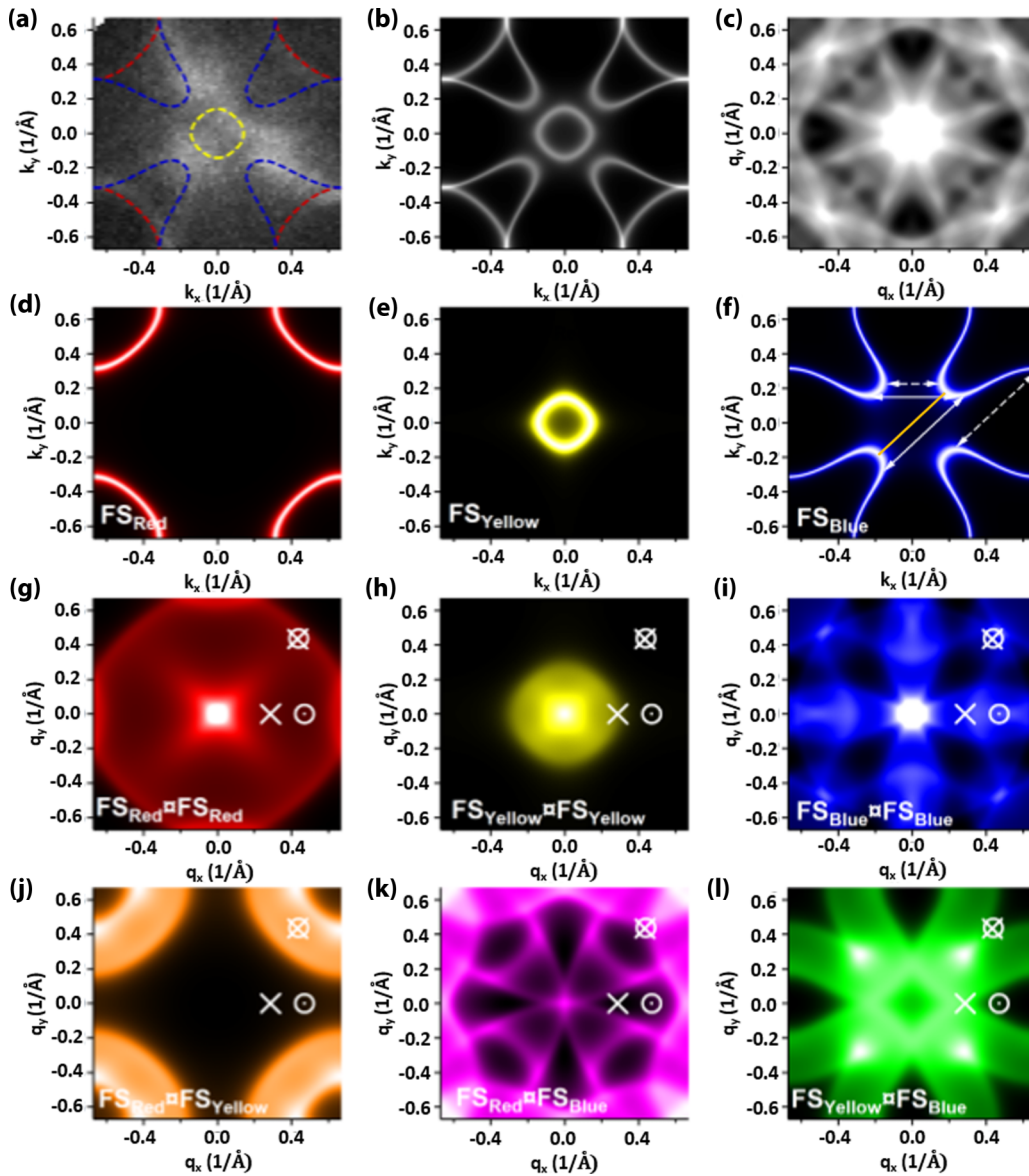
FIG. 5. (a) Our experimentally measured Fermi surface is overlaid with our TB parametrization of Eq. (1). (b) The idealized Fermi surface obtained from our TB parametrization. (c) Complex q-space structure obtained by autocorrelating the Fermi surface in (b). (d)–(f) Three components that make up the full Fermi surface shown in (b). (g)–(i) Autocorrelations of Fermi surface in (d)–(f) showing the q vectors associated with intraband scattering. (j)–(l) The same as (g)–(i) but now the correlations reflect interband scattering as indicated. In (g)–(i) and (j)–(l) the critical q vectors determined in Ref. [16] are indicated by conduction band q vector (circle) and the superconducting gap q vector (×). The most likely scattering q vectors are also shown by the arrows in panel (f), solid lines correspond to the conduction band from Refs. [16,17], and the dashed lines to the superconducting gap from Ref. [18]. The yellow line indicates a third critical q vector connecting the conduction bands from Ref. [17].

between the Ce $4f$ electons and the itinerant In $5p$ band. Thus, at the simplest level one might associate such an interaction with the two-dimensional (2D) CeIn$_3$ planes, bringing this superconductor into alignment with the related unconventional superconductors, the cuprates and the pnictides, where the two-dimensionality is thought to play an important role in the high superconducting transition temperatures. The present study, however, suggests a picture whereby the pairing in CeCoIn$_5$ reflects hybridization with the out-of-the-plane In atoms and neighboring Co atoms in the CoIn$_2$ planes and points to a more 3D superconductor [4,9]. Indeed, the involvement of electrons in the CoIn$_2$ planes would indicate a more

significant role for the localized Co $3d$ electrons. Interestingly, support for this concept is given by the observation that substituting Ir and Rh for the Co atoms results in a reduction in T_c in the case of the more itinerant Ir and the replacement of superconductivity by antiferromagnetism as the ground state in the case of the more localized Rh [1,5].

[1] B. D. White, B. D. J. D. Thompson, and M. B. Maple, Phys. C (Amsterdam, Neth.) **514**, 246 (2015).

[2] C. Petrovic, P. Pagliuso, M. Hundley, R. Movshovich, J. Sarrao, J. Thompson, Z. Fisk, and P. Monthoux, J. Phys.: Condens. Matter **13**, L337 (2001).

[3] T. Maehira, T. Hotta, K. Ueda, and A. Hasegawa, J. Phys. Soc. Jpn. **72**, 854 (2003).

[4] J. H. Shim, K. Haule, and G. Kotliar, Science **318**, 1615 (2007).

[5] K. Haule, C.-H. Yee, and K. Kim, Phys. Rev. B **81**, 195107 (2010).

[6] G. R. Stewart, Rev. Mod. Phys. **56**, 755 (1984).

[7] H. C. Choi, B. I. Min, J. H. Shim, K. Haule, and G. Kotliar, Phys. Rev. Lett. **108**, 016402 (2012).

[8] A. Damascelli, Z. Hussain, and Z. X. Shen, Rev. Mod. Phys. **75**, 473 (2003).

[9] A. Koitzsch, S. V. Borisenko, D. Inosov, J. Geck, V. B. Zabolotnyy, H. Shiozawa, M. Knupfer, J. Fink, B. Büchner, E. D. Bauer, J. L. Sarrao, and R. Follath, Phys. Rev. B **77**, 155128 (2008).

[10] A. Koitzsch, I. Opahle, S. Elgazzar, S. V. Borisenko, J. Geck, V. B. Zabolotnyy, D. Inosov, H. Shiozawa, M. Richter, M. Knupfer, J. Fink, B. Büchner, E. D. Bauer, J. L. Sarrao, and R. Follath, Phys. Rev. B **79**, 075104 (2009).

[11] A. Koitzsch, T. K. Kim, U. Treske, M. Knupfer, B. Büchner, M. Richter, I. Opahle, R. Follath, E. D. Bauer, and J. L. Sarrao, Phys. Rev. B **88**, 035124 (2013).

[12] J. Xiao-Wen *et al.*, Chin. Phys. Lett. **28**, 057401 (2011).

[13] Q. Y. Chen, D. F. Xu, X. H. Niu, J. Jiang, R. Peng, H. C. Xu, C. H. P. Wen, Z. F. Ding, K. Huang, L. Shu *et al.*, Phys. Rev. B **96**, 045107 (2017).

[14] K. Kummer, S. Patil, A. Chikina, M. Güttler, M. Höppner, A. Generalov, S. Danzenbächer, S. Seiro, A. Hannaske, C. Krellner *et al.*, Phys. Rev. X **5**, 011028 (2015).

[15] P. Aynajian, E. H. da Silva Neto, A. Gyenis, R. E. Baumbach, J. D. Thompson, Z. Fisk, E. D. Bauer, and A. Yazdani, Nature **486**, 201 (2012).

[16] M. P. Allan, F. Massee, D. K. Morr, J. Van Dyke, A. W. Rost, A. P. Mackenzie, C. Petrovic, and J. C. Davis, Nat. Phys. **9**, 468 (2013).

[17] B. B. Zhou, S. Misra, E. H. da Silva Neto, P. Aynajian, R. E. Baumbach, J. D. Thompson, E. D. Bauer, and A. Yazdani, Nat. Phys. **9**, 474 (2013).

[18] J. S. Van Dyke, F. Massee, M. P. Allan, J. C. S. Davis, C. Petrovic, and D. K. Morr, Proc. Natl. Acad. Sci. USA **111**, 11663 (2014).

[19] M. Mansson, T. Claesson, U. O. Karlsson, O. Tjernberg, S. Pailhs, J. Chang, J. Mesot, M. Shi, L. Patthey, N. Momono, M. Oda, and M. Ido, Rev. Sci. Instrum. **78**, 076103 (2007).

[20] A. Sekiyama, T. Iwasaki, K. Matsuda, Y. Saitoh, Y. Onuki, and S. Suga, Nature **403**, 396 (2000).

[21] See Supplemental Material at http://link.aps.org/supplemental/10.1103/PhysRevB.102.205112 for the superconducting pairing mechanism in CeCoIn$_5$ revisited.

[22] P. Blaha, K. Schwarz, P. Sorantin, and S. B. Trickey, Comput. Phys. Commun. **59**, 399 (1990).

[23] P. Blaha, K. Schwarz, G. Madsen, D. Kvasnicka, and J. Luitz (Technische Universitaet Wien, Vienna, Austria, 2001).

[24] B. Barbiellini, E. G. Moroni, and T. Jarlborg, J. Phys.: Condens. Matter **2**, 7597 (1990).

[25] J. P. Perdew, K. Burke, and M. Ernzerhof, Phys. Rev. Lett. **77**, 3865 (1996).

[26] T. Nomoto and H. Ikeda, Phys. Rev. B **90**, 125147 (2014).

Correction: The previously published Figure 5 contained an omission of scale numbers and has been replaced.